PB82-154717

Monte Carlo Simulation of Daily Regional Sulfur Distribution: Comparison with SURE Sulfate Data and Visual Range Observations during August 1977

Washington Univ.
St. Louis, MO

Prepared for

Environmental Sciences Research Lab.
Research Triangle Park, NC

13 Jan 81

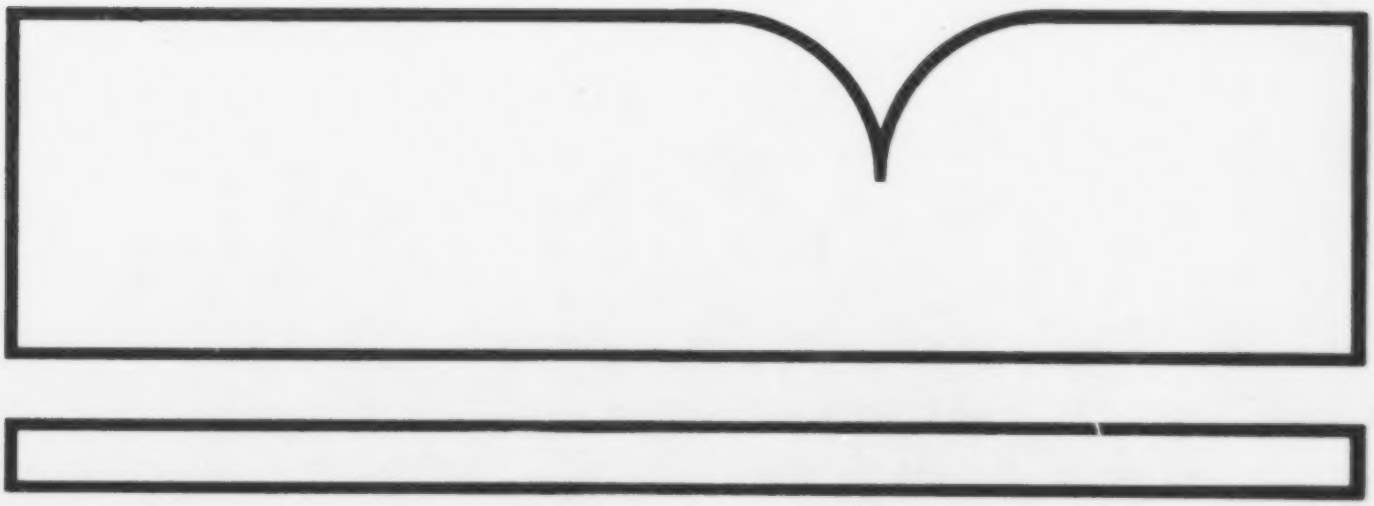

U.S. Department of Commerce
National Technical Information Service
NTIS.

TECHNICAL REPORT DATA
(Please read Instructions on the reverse before completing)

1. REPORT NO. EPA-600/J-81-056	2. Journal Article	3. PB82-154717
4. TITLE AND SUBTITLE MONTE CARLO SIMULATION OF DAILY REGIONAL SULFUR DISTRIBUTION: Comparison with SURE Sulfate Data and Visual Range Observations During August 1977		5. January 1982 6. PERFORMING ORGANIZATION CODE 029062
7. AUTHOR(S) D.E. Patterson, R.B. Husar, W.E. Wilson, and L.F. Smith		8. PERFORMING ORGANIZATION REPORT NO.
9. PERFORMING ORGANIZATION NAME AND ADDRESS Center for Air Pollution Impact and Trend Analysis Washington University St. Louis, MO 63130		10. PROGRAM ELEMENT NO. CDTA1D/02-0218 (FY-81) 11. CONTRACT/GRANT NO.
12. SPONSORING AGENCY NAME AND ADDRESS Environmental Sciences Research Laboratory - RTP, NC Office of Research and Development U.S. Environmental Protection Agency Research Triangle Park, N.C. 27711		13. TYPE OF REPORT AND PERIOD COVERED 14. SPONSORING AGENCY CODE EPA/600/09

15. SUPPLEMENTARY NOTES
REFERENCE: J. Applied Meteorology, 20:70-86, April 1981.

16. ABSTRACT

The daily distribution of sulfate concentration over the eastern United States during August 1977 is simulated by a Monte Carlo model using quantized emissions, positioned in accordance with the 1973 EPA SO_2 emission inventory. Horizontal advection within a single well-mixed vertical layer is driven by observed surface winds, speeded by a factor of 2.5 and veered 20°. Direct simulation of regional diffusion is implemented by random perturbation of each quantum's trajectory over each 3 h timestep, corresponding to $K = 10^5 m^2 s^{-1}$. First order kinetics of SO_2 to $SO_4^=$ transformation and deposition of SO_2 and $SO_4^=$ are simulated by probabilistic choice among the chemical and physical pathways over each step. The simulated spatial distributions are compared on a daily basis to measured sulfate concentration from the Sulfate Regional Experiment (SURE) and midday visual range observations, indicating the primary role of airmass residence time over the eastern United States in producing regional pollution. The light extinction coefficient, b_{ext}, and SURE $SO_4^=$ show remarkable spatial and temporal agreement throughout the month. The correlations of daily average $SO_4^=$ concentration and b_{ext} over the SURE region with the Monte Carlo simulation are 0.63 and 0.67, respectively. The correlation between daily average b_{ext} and measured $SO_4^=$ is 0.84.

17. KEY WORDS AND DOCUMENT ANALYSIS

a. DESCRIPTORS	b. IDENTIFIERS/OPEN ENDED TERMS	c. COSATI Field/Group

18. DISTRIBUTION STATEMENT RELEASE TO PUBLIC	19. SECURITY CLASS (This Report) UNCLASSIFIED	21. NO. OF PAGES
	20. SECURITY CLASS (This page) UNCLASSIFIED	22. PRICE

REPRODUCED BY NATIONAL TECHNICAL INFORMATION SERVICE U.S. DEPARTMENT OF COMMERCE SPRINGFIELD, VA 22161

EPA-600/J-81-056
Journal Article

Monte Carlo Simulation of Daily Regional Sulfur Distribution: Comparison with SURE Sulfate Data and Visual Range Observations during August 1977

D. E. PATTERSON AND R. B. HUSAR

Center for Air Pollution Impact and Trend Analysis (CAPITA), Washington University, St. Louis, MO 63130

W. E. WILSON

Regional Field Studies Office, U.S. EPA, Research Triangle Park, NC 27711

L. F. SMITH

Office of Energy Research, U.S. EPA, Washington, DC 20460

(Manuscript received 5 August 1980, in final form 13 January 1981)

ABSTRACT

The daily distribution of sulfate concentration over the eastern United States during August 1977 is simulated by a Monte Carlo model using quantized emissions, positioned in accordance with the 1973 EPA SO_x emission inventory. Horizontal advection within a single well-mixed vertical layer is driven by observed surface winds, speeded by a factor of 2.5 and veered 20°. Direct simulation of regional diffusion is implemented by random perturbation of each quantum's trajectory over each 3 h time step, corresponding to $K = 10^5$ m^2 s^{-1}. First order kinetics of SO_2 to $SO_4^=$ transformation and deposition of SO_2 and $SO_4^=$ are simulated by probabilistic choice among the chemical and physical pathways over each step. The simulated spatial distributions are compared on a daily basis to measured sulfate concentration from the Sulfate Regional Experiment (SURE) and midday visual range observations, indicating the primary role of airmass residence time over the eastern United States in producing regional pollution. The light extinction coefficient, b_{ext} and SURE $SO_4^=$ show remarkable spatial and temporal agreement throughout the month. The correlations of daily average $SO_4^=$ concentration and b_{ext} over the SURE region with the Monte Carlo simulation are 0.63 and 0.67, respectively. The correlation between daily average b_{ext} and measured $SO_4^=$ is 0.84.

1. Introduction

It is now widely accepted that the tropospheric lifetime of fine particulates such as sulfates is typically 3–5 days at midlatitudes (*International Symposium on Sulfur in the Atmosphere*, 1978). Such pollutants, therefore, may be transported for distances well in excess of 1000 km after emission, mingling with numerous other plumes to create regional scale areas of high concentration (e.g., Hidy *et al.*, 1978; Wolff *et al.*, 1977). The difficulty of identifying the sources of fine particles at any receptor site lead to the use of diagnostic long-range transport models, such as that of the European Organization for Economic Cooperation and Development (OECD), (Eliassen, 1978).

The purpose of our work is to develop a conceptually and computationally simple[1] approach for daily simulation of regional-scale pollutant distribution. The model incorporates the major processes involved in the atmospheric transmission of pollutants: transport, chemical transformations and deposition to surfaces. It is to be used as a diagnostic tool to unravel some of the complexities of regional source-receptor relationships. An early version of the model is described and the simulation is compared to measured concentration distributions of sulfate and haziness in the eastern United States during August 1977.

2. Data

Data from two sources were used. The Sulfate Regional Experiment (SURE), (Perhac, 1978), conducted by Environmental Research and Technology, Inc., for the Electric Power Research Institute (EPRI), measured daily average sulfate concentration at 49 sites (Fig. 1b) in the eastern United States during August 1977. Midday observations of visual range, relative humidity, pressure, and surface wind direction and surface wind speed for the month were

[1] The model is currently implemented on a PDP 11/45 minicomputer.

0021-8952/81/000000-00500.00

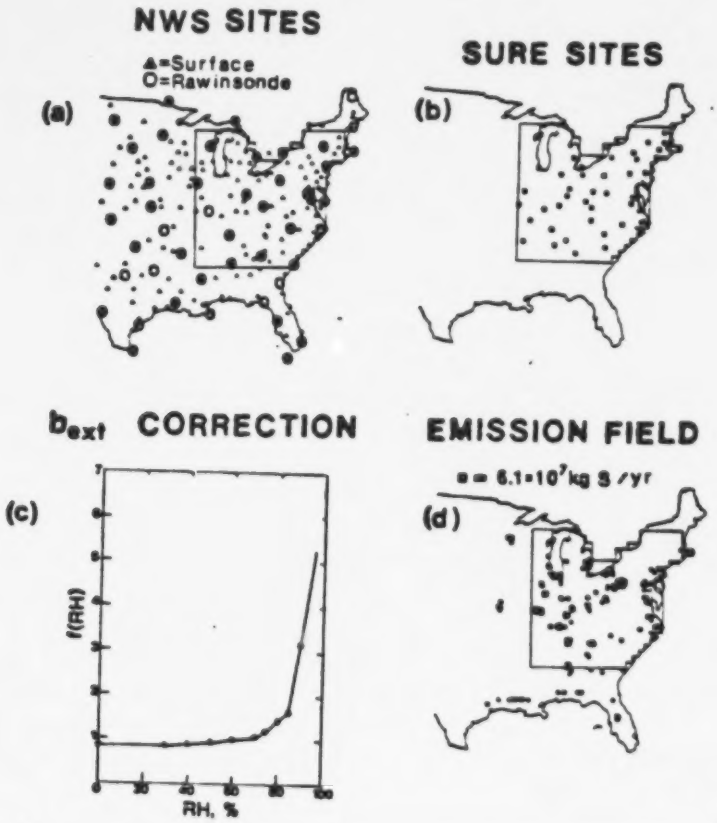

FIG. 1. (a) Location of National Weather Service sites which report visual range, relative humidity and surface winds. Circled locations indicate the rawinsonde sites. (b) Location of SURE sulfate sites. Squared boundary indicates the maximum extent of the SURE region for computation of spatial averages. (c) Functional form used to normalize the extinction coefficient to 60% RH. (d) SO_2 quanta emission inventory used in the simulation.

obtained for 178 National Weather Service sites (Fig. 1a): the *Federal Meteorological Handbook* (1975) details the observational methods. Visual range observations (in miles) provide an estimate of haziness via the Koschmieder relationship b_{ext} = 24/visual range, where the light extinction coefficient b_{ext} has units of 10^{-4} m^{-1}. A further modification was performed to normalize b_{ext} to 60% RH: $b_{ext}(60\%) = b_{ext}/f(\mathrm{RH})$. The functional form of $f(\mathrm{RH})$ is illustrated in Fig. 1c; b_{ext} in what follows refers to the normalized value. The correction, in practice, has little effect other than to reduce the weighting of precipitation-influenced visibility observations at midday. The empirical correction curve $f(\mathrm{RH})$ was constructed subjectively using laboratory data on the RH dependence of aerosol light scattering (Covert *et al.*, 1972), as well as visibility-RH relationships from various sites. The actual spatial and temporal behavior of $f(\mathrm{RH})$ depends on aerosol chemistry and size distribution and is not available.

The data for all reporting sites for each parameter were interpolated onto a square grid with 60 km spacing via the weighting

$$V_{ij} = \sum_k V(k) r_{ij}^{-2}(k) / \sum_k r_{ij}^{-2}(k),$$

where $V(k)$ are the data at site k and $r_{ij}(k)$ is the distance from site k to grid point ij. Each grid point weighs data from about 3 to 6 of the nearest National Weather Service sites. A further smoothing was applied to the grid:

$$V_{ij}' = (4V_{ij} + V_{ij-1} + V_{ij+1} + V_{i-1j} + V_{i+1j})/8.$$

Grid points lying outside the United States map boundaries were eliminated to avoid extrapolation errors. The wind vector components northward and eastward were gridded and smoothed separately. Each SURE site was assigned to the nearest National Weather Service location for gridding calculations; maximum dislocation was <60 km. For all

parameters except wind speed, a northeastern United States spatial average was computed as the mean of all grid values lying on or within the SURE region in Fig. 1b.

3. Description of the Monte Carlo simulation

The Monte Carlo approach to simulation of physical and chemical atmospheric processes has the following key characteristics: 1) each process (transport, transformation, deposition) is simulated directly as a discrete event; 2) mass conservation is maintained by counting each pollutant quantum as it moves and changes chemical form, rather than via differential equations; and 3) direct Monte Carlo simulation is Lagrangian since trajectories of individual quanta are followed, but Eulerian in that in the limit of an infinite number of quanta and infinitesimal time step a stochastic solution of a two-dimensional diffusion equation with nonsteady-state inhomogeneous flow is obtained. Its Lagrangian features are most useful for simulation of kinetics; the Eulerian aspects benefit the transport simulation.

The simulation is stochastic for both the diffusion and the transformation-removal kinetics. Emissions are simulated as a number of quantum masses of pollutant, each located at one geographic point at each time step. Regional diffusion is implemented by randomly perturbing individual trajectories for direct simulation of diffusion. The Monte Carlo approach to diffusion in the mesoscale is well documented in literature (e.g., Hall, 1975; Alsmiller *et al.*, 1979), although it is not common in regional-scale models. Kinetics of chemical transformation and dry and wet deposition are imposed as stochastic events during each time step rather than via differential equations. Hence, at each time step each emitted quantum mass of sulfur is considered to be *entirely* in one form: either primary SO_2, secondary $SO_4^=$, or previously deposited sulfur. These aspects make it possible to maintain a time history of the simulated location and physical-chemical form of every emission quantum, such as required for source-receptor budgeting. Table 1 summarizes the current model implementation.

a. Emissions

For eastern United States annual SO_2 emissions of 25×10^9 kg year^{-1}, each of the 204 quanta emission sources used in this application represent 6.1 $\times 10^7$ kg S year^{-1} or 2.1×10^4 kg S (3 h)$^{-1}$ time step between simulated emissions. Sources outside the region, such as in the western United States and Canada, are not considered. The density and position of quantum mass sources (Fig. 1d) is in accordance with the U.S. EPA's 1973 SO_2 emission inventory by air quality control region (AQCR). Many AQCR's with small emissions are not allocated any

TABLE 1. Model formulation.

Component	Approach	Current implementation
Emissions	Quantized point mass	Based on EPA SO_2 inventory, 204 quanta, emitted every 3 h, unit mass 2.1×10^4 kg S.
Advection	Horizontal flow only, in well-mixed vertical layers	Single vertical layer, advecting winds from gridded, modified midday surface wind observations, 3 h time step, limited to United States boundaries.
Diffusion	Random horizontal displacement, simulating eddy diffusion, vertical wind shear	Displacement of radius 46 km with random direction every 3 h, following advection time step.
Kinetics	Probabilistic choice among pathways over each time step, given transition probabilities (P) which may be extracted from rate constants (k) via $P = 1 - e^{-k\Delta t}$	3 h time step, rates constant in space and time. Pathways: $SO_2 \rightarrow SO_4^=$ ($P_r = 0.038$, $k_r = 0.013$ h^{-1}); $SO_2 \rightarrow$ wet and dry SO_2 deposition ($P_r = 0.100$, $k_r = 0.035$ h^{-1}); $SO_2 \rightarrow SO_2$ ($P_s = 1 - P_r - P_r = 0.862$); $SO_4^= \rightarrow$ wet and dry $SO_4^=$ deposition ($P_d = 0.044$, $k_d = 0.015$ h^{-1}); $SO_4^= \rightarrow SO_4^=$ ($1 - P_d = 0.956$)
Model output	Vertical integral of pollutants at points in horizontal plane at each time step, deposition over a time step	Superposition of eight time step's output onto daily average 60 km grid, spatial smoothing, surface concentration estimate by assuming 1100 m perfectly mixed vertical layer at all points in space and time
Comparison to data	Daily average spatial patterns	Gridded daily average $SO_4^=$ surface concentration, based on SURE measurements during August 1977, and gridded midday b_{ext} values from visual range observations

emissions; the multiple quanta were positioned subjectively within each AQCR. In Section 5 evidence that this simulation is rather insensitive to the spatial distribution of emission sources is presented.

b. Advection

In the current application only horizontal transport is explicitly considered; the simulation assumes that the pollutant is confined within a single well-mixed vertical layer. Due to the absence of wind data, trajectories which exit the United States are terminated. However, transport toward the western half of the country and recirculation back to the east is permissible in the simulation. We have chosen to use modified midday surface winds for horizontal advection. Due to intensive mixing, vertical wind shear (both speed and directional effects) are at a minimum during summer afternoons, so that midday surface winds are coupled to the synoptic flow. Surface winds are less representative of mean advecting winds than upper air soundings at the 19 rawinsonde sites in the SURE region. However, the surface winds offer a 4–5 times denser network, and hence better spatial resolution. Pack *et al.* (1978) have described trajectory comparisons in which modified surface winds predicted tetroon motion better than either geostrophic winds or measured upper air winds. The relationship of surface winds to mean boundary-layer advecting winds also has been addressed by Counihan (1975), Smith and Jeffrey (1975) and Maul (1978).

Temporal resolution of midday surface wind fields is coarser than the 12 h (morning and evening) resolution of upper air observations; nighttime surface winds are often decoupled from winds aloft. The existence of summertime low-level jets overnight in the midwest (Bonner *et al.*, 1968; Smith *et al.*, 1978) may be an important factor in long-range transport which is not detected by either upper air or surface wind networks.

Trajectories of modified surface winds were calibrated in two ways: comparison to upper air trajectory calculations and by comparison to the motion of hazy airmasses. Using a constant velocity numerical integration scheme, trajectories were computed from gridded midday winds by varying the veer and wind-speed scale factor. Calibration indicated that the best match to selected 4-day upper air trajectories calculated by the method of Heffter *et al.* (1975) during periods in June and July 1975 was obtained with veer 20° clockwise in the direction of motion and wind-speed scale factor 2.5. The observed surface winds, modified as above, were then used to generate trajectories for comparison with the observed motion of a large-scale hazy airmass during 23 June–5 July 1975. The modified surface wind transport provided acceptable agreement to the apparent motion, and was therefore adopted.

Fig. 2 shows another comparison of 4-day back trajectories estimated via the method of Heffter *et al.* (1975) and by the modified surface wind scheme for four successive days in July 1977. The trajectories arriving in St. Louis, Missouri, on 15 July are very similar. The two trajectories arriving on 16 and 17 July are very dissimilar, with our method indicating recirculation within the midwest while the Heffter calculations indicate a reasonably direct flow from the Gulf. The contours of the light extinction coefficient b_{ext} would indicate a regional stagnation east of St. Louis during this period but do not seem to indicate a basis for preferring either trajectory method. The trajectories arriving on 18 July also differ considerably. For simulation of horizontal advection, the higher spatial resolution of surface wind observations motivated their use. Presumably, a judicious combination of information from these alternative sources would be an improved technique.

c. Diffusion

Clearly, simulation of long-range transport is limited by the accuracy of airmass trajectory computations. Unfortunately, the concept of "the trajectory" of an air parcel during multiday transport has no physical realization. After repeated subjection to diurnal planetary boundary-layer dynamics of turbulent diffusion, oscillations in mixing height and vertical wind shear, a puff of emitted material may be dispersed beyond recognition into part of a large-scale "background' airmass. The spreading effect is implemented by superimposing a perturbation on the advecting trajectory at each time step of integration. The perturbation should, ideally, reflect the climatological value of horizontal regional-scale "diffusivity" as a geographical function of time of day, based on upper air wind characteristics (e.g., Samson, 1978, 1980) and multiday plume measurements.

For computational simplicity, the diffusion is currently simulated by an effective diffusion coefficient K such that a displacement of radius $\sqrt{2K\Delta t}$ is imposed with randomly chosen direction following the advection step. Values of K from 10^2–10^6 m^2 s^{-1} have been used in models on the mesoscale (representing eddy diffusivity) to global scale (Munn and Bolin, 1971).

The role of diffusion from an Eulerian and Lagrangian point of view is illustrated in Fig. 3, which shows 100 randomized trajectories with $K = 10^5$ m^2 s^{-1} and the unrandomized trajectory (heavy line) originating from each of two point sources on 1 August 1977. All trajectories from each source have the same initial location and time of release, and are advected by the same time-varying two-dimensional wind field, differing only in the sequence of random perturbations that each undergoes. The trajectories from the source in Fig. 3a lie clustered about the

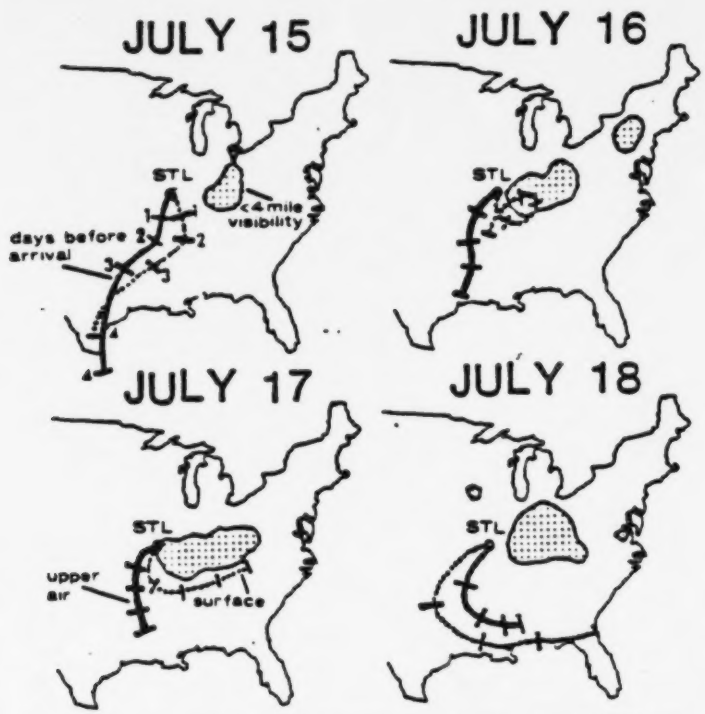

FIG. 2. Four-day back trajectories arriving at St. Louis, Missouri (STL) on 15, 16, 17 and 18 July 1977. Tick marks are at 24 h intervals.

nonrandomized trajectory. Hence, the unrandomized trajectory is a good representation of the mean transport field, since the crosswind dispersion about it can be described by a Gaussian distribution. However, the trajectories in Fig. 3b indicate a wide range of dispersion, with many trajectories from this source diffusing into an advecting wind regime that carries them far to the west of the unperturbed flow. Fig. 3b

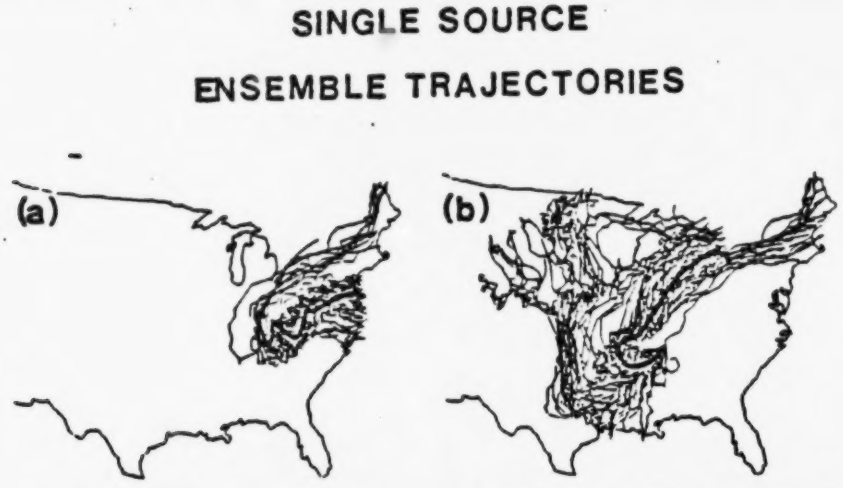

FIG. 3. The effect of eddy diffusion coefficient $K = 10^6$ m^2 s^{-1} is illustrated by 100 sample trajectories from a single source. The unperturbed trajectory is represented by the heavy line ($K = 0$). The scatter in trajectories is created by the individual sequence of random perturbations in combination with the spatially nonhomogeneous flow field.

demonstrates the advantage of an Eulerian view, namely, that the diffusion in a heterogeneous flow field leads to non-Gaussian dispersion. In the limit of large numbers of quanta, the Monte Carlo approach is both Lagrangian and Eulerian. In the model simulation, only one trajectory is chosen, so that the single quantum emitted at the source in Fig. 3b might be exported to the Great Lakes within 3–4 days or remain in the Rocky Mountain states after 10 days, depending on the sequence of random diffusion steps it experiences.

The value of $K = 10^5$ m^2 s^{-1} was chosen by inspection to yield acceptable regional dispersion and avoid the problem of excessive clustering. An order-of-magnitude test for the value of K was performed, using the quantized SO_2 emissions as conservative tracers (Figs. 4a–d). With $K = 0$, distinct clusters of quanta indicate convergent flow. Taking $K = 10^4$ m^2 s^{-1} still leads to excessive clustering, compared to observed sulfate (Fig. 7). The general features of the simulated spatial distribution are preserved without distinct plumes if a value of $K = 10^5$ m^2 s^{-1} is assumed, but $K = 10^6$ m^2 s^{-1} causes an overly uniform simulated spatial distribution.

d. Kinetics

The kinetic actions of SO_2 deposition, SO_2 to $SO_4^=$ transformation, and $SO_4^=$ deposition are imposed subsequent to the transport calculation step. The discrete nature of emission quanta permits examination of multiple kinetic scenarios (without recalculation of trajectories) from the time and position history of each quanta, assuming only that kinetics can be specified in terms of probabilities of transformation and removal at every point in space and time. This Monte Carlo kinetic technique permits inclusion of externally supplied rates of wet removal, as well as quite general parameterizations of other rate constants. At each time step, each quantum emission unit is flagged as being either SO_2, $SO_4^=$, wet/dry deposited $SO_2/SO_4^=$, or exported $SO_2/SO_4^=$.

SO_2 may undergo conversion to $SO_4^=$ or be dry or wet deposited, while $SO_4^=$, once formed, is subject to removal only (Fig. 5a). The possible paths for SO_2 and the associated transition probabilities are conversion to $SO_4^=$ (P_t), deposition (P_r), and continuation as SO_2 [$P_0 = 1 - (P_t + P_r)$]; for $SO_4^=$ the kinetic paths are deposition (P_d) or continuation as

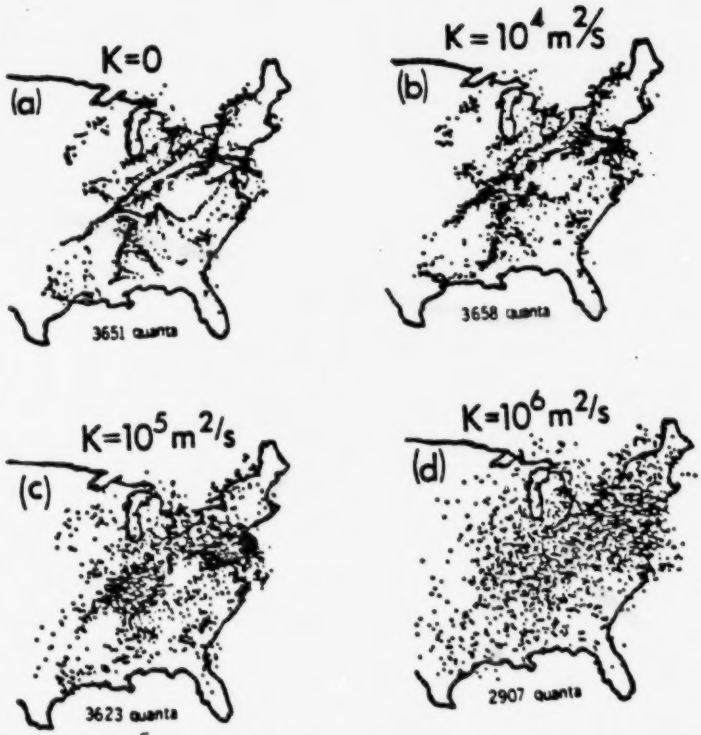

FIG. 4. Result of transport calculations with continuous emissions from 28 July–3 August 1977, using eddy diffusion coefficients of (a) 0, (b) 10^4 m^2 s^{-1}, (c) 10^5 m^2 s^{-1}, (d) 10^6 m^2 s^{-1}.

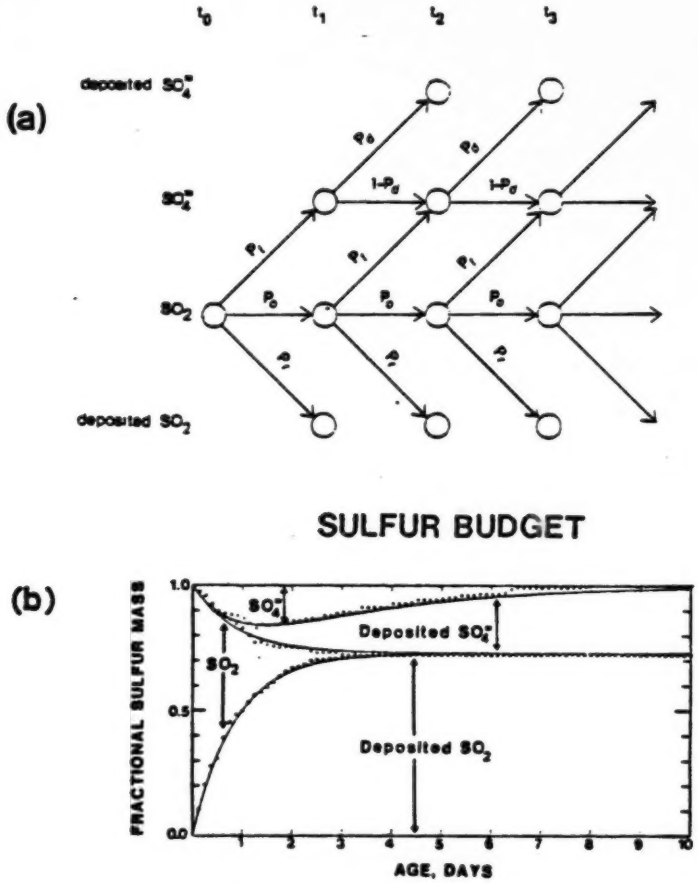

FIG. 5. (a) Schematics of probabilistic decisions for the simulation of kinetics. (b) Analytic sulfur budget (curves) and a sample stochastic simulation budget of 204 quanta (points), arising from probabilities used in this application.

$SO_4^=$ $(1 - P_d)$. Choice of the kinetic path for each quantum at each time step is implemented by dividing the interval (0, 1) into subintervals: for SO_2, the ranges $(0, P_t]$[2], $(P_t, P_t + P_r]$ and $(P_t + P_r, 1)$ correspond to $SO_4^=$ formation, SO_2 deposition, and continuation as SO_2; $(0, P_d]$ and $(P_d, 1)$ define $SO_4^=$ deposition and continuation as $SO_4^=$. A random number from the uniform distribution on (0, 1) falls within one of the subintervals, causing the corresponding simulated kinetic action.

In this application, the rate constants are invariant in space and time, with average dry and wet deposition combined. Following the results of the OECD study (Eliassen, 1978), we have taken the rates of SO_2 – $SO_4^=$ conversion, SO_2 total deposition and $SO_4^=$ total deposition to be 0.013, 0.035 and 0.015 h^{-1}, respectively. Over the period Δt = 3h, the probabilities are related to the rate constants k as $P = 1 - \exp(-k\Delta t)$. Thus the rate constants above correspond to probabilities of kinetic action over a 3 h period of 0.038, 0.100 and 0.044, respectively. The corresponding sulfur budget with time is shown in Fig. 5b.

Fig. 6 illustrates the overall model simulation. The regional-scale trajectory arises from advection via modified surface winds combined with random perturbations, and subsequent kinetic simulation. The thin lines of the early quantum emission's history denote continuation as SO_2. The change to thick lines indicates the kinetic path of conversion of the entire quantum's mass to $SO_4^=$. The end of the thick line reflects deposition as $SO_4^=$. The dotted path is the remainder of the calculated trajectory to the point of export beyond the U.S. boundary. The encircled trajectory segment depicts each step in detail: ad-

[2] The interval notation is such that parentheses correspond to > or <, while square brackets correspond to ≥ and ≤.

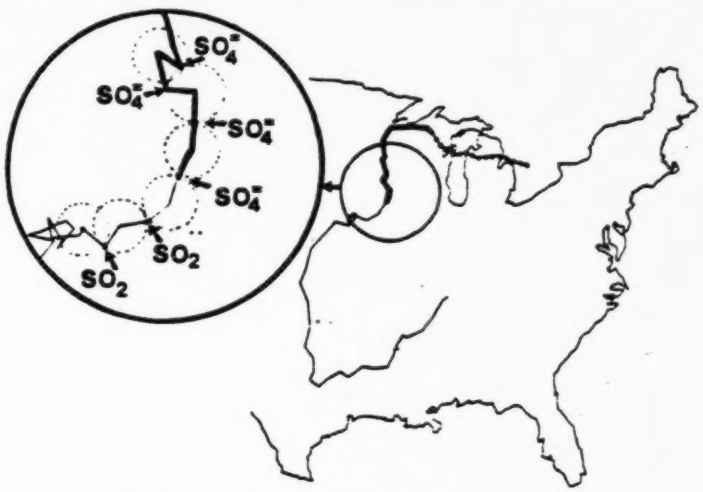

FIG. 6. Overall stochastic simulation of transport, transformation and removal applied to one quantum. Detail shows each model component: advection, random perturbation about a circle, kinetic decision over each time step.

vecting flow, random dislocation onto a circle, and stochastic kinetic decisions at each step.

4. Simulation of August 1977

a. Daily maps

Contour plots of EPRI-SURE daily average $SO_4^=$ concentration distribution are compared to corresponding simulated sulfate fields within the SURE sampling region. The simulation, assuming an initial condition of *no* atmospheric sulfur, was initiated on 26 July to achieve a quasi-steady state by 1 August. For contouring purposes, the simulated sulfate mass over each grid area was expressed in concentration units by assuming a uniform scale height of 1100 m, which is the average ratio of simulated burden to observed concentration. Figs. 7–11 depict (in columns from left to right) the light extinction coefficient normalized to 60% RH, measured daily average $SO_4^=$ concentration (the dots are reporting SURE sites), the simulated $SO_4^=$ distribution, and the surface wind field superimposed on the sea level pressure distribution. The thin squared boundaries indicate the SURE region over which the spatial averages were computed; the averages are shown in the numbers above the maps. Note that the region of spatial averaging is slightly smaller on 3, 4 and 6 August due to lack of SURE data at outlying sites.

On the first day of the sampling program, sulfate levels above 10 $\mu g\ m^{-3}$ were observed only on the eastern seaboard, with New England experiencing 15–20 $\mu g\ m^{-3}$. Haze, with noon visibility < 6 mi, was also confined to the seaboard, as was the simulated sulfate. The synoptic meteorology was characterized by a high-pressure system in the midwest and an eastward moving cold front. On 1 August, most of the observed and simulated sulfates were east of the front. By 2 August, the front had passed over New England, sweeping the sulfates and haze to the Atlantic. In the same time period, stagnation from Missouri to Ohio resulted in the accumulation of emissions on 2 and 3 August. By 3 August, sulfate levels exceeded 20 $\mu g\ m^{-3}$ in large parts of West Virginia and Ohio.

For the following five days, 4–8 August, a high-pressure system resided over South Carolina, Georgia and Alabama, causing stagnation within those states and the familiar clockwise circulation around the high, which transported the accumulated emissions in the midwest to New England and Canada on 4 August and to the Atlantic on 5 August.

Between 10 and 15 August, the eastern U.S. ventilation decreased somewhat, resulting in pockets of sulfate and haze over one or two state areas, with fair to poor spatial correspondence between simulated and measured levels. For 15 August, a spatial mismatch between SURE sulfate data and haziness on one hand and the Monte Carlo simulation on the other should be noted. On 16–18 August, a fast moving Canadian front advanced over most of the eastern United States, sweeping the accumulated pollutants to the east and southeast to the Atlantic. The observed $SO_4^=$ levels, haziness and Monte Carlo simulation all show the clearing of the region on the 18th.

For a full week, between 19 and 26 August, eastern United States ventilation was poor, as evidenced by the low wind speeds from 19–23 August, and was further decreased by the approaching high pressure system on the 24th, 25th and 26th. As usual,

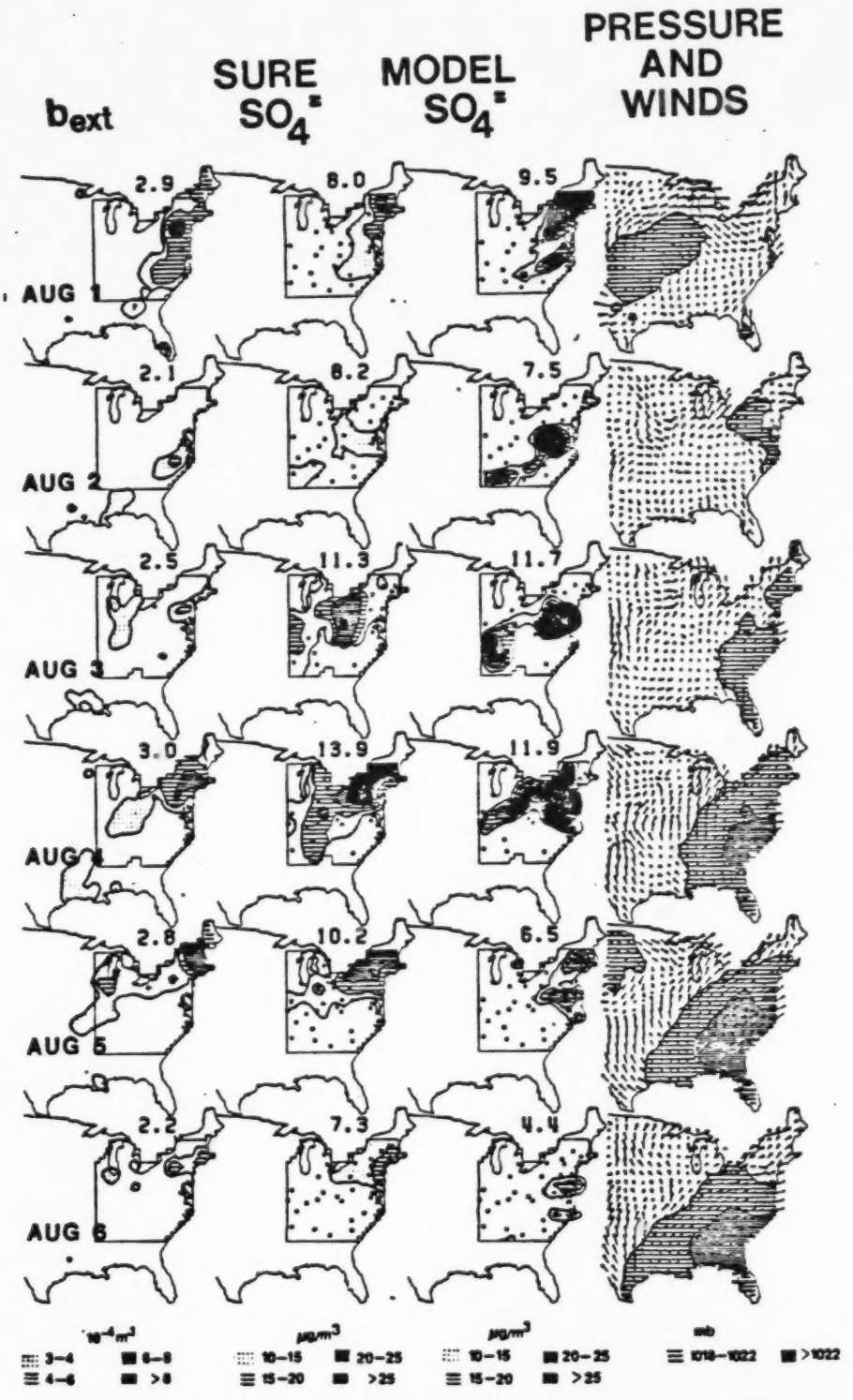

FIG. 7. Daily maps of midday b_{ext} corrected to 60% RH (first column), 24 h average SURE $SO_4^=$ (2nd column), modeled 24 h distribution of emitted sulfur quanta (third column), and unmodified noon surface wind field overlaid with the sea level pressure (last column) for 1–6 August 1977.

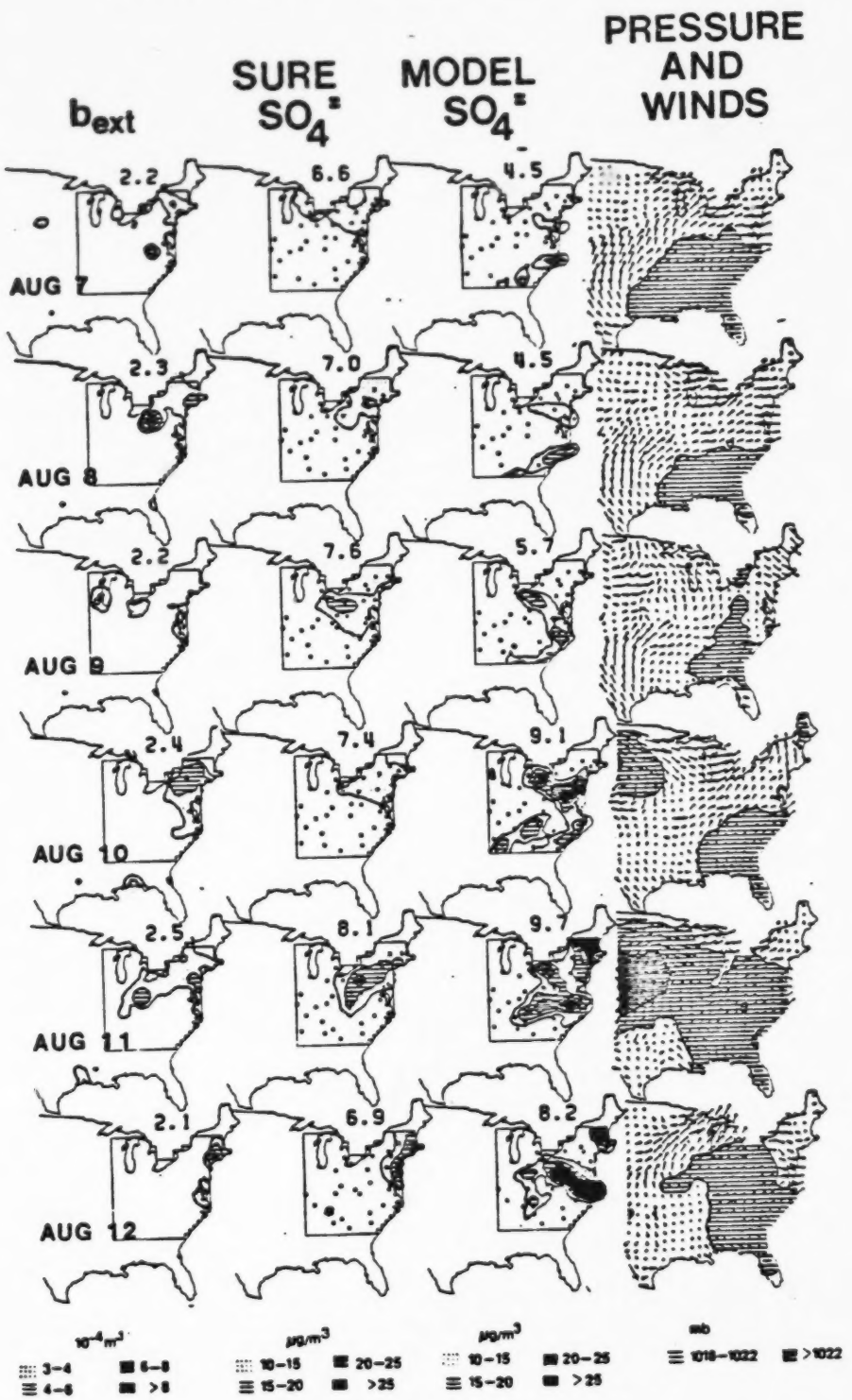

FIG. 8. As in Fig. 7 except for 7–12 August 1977.

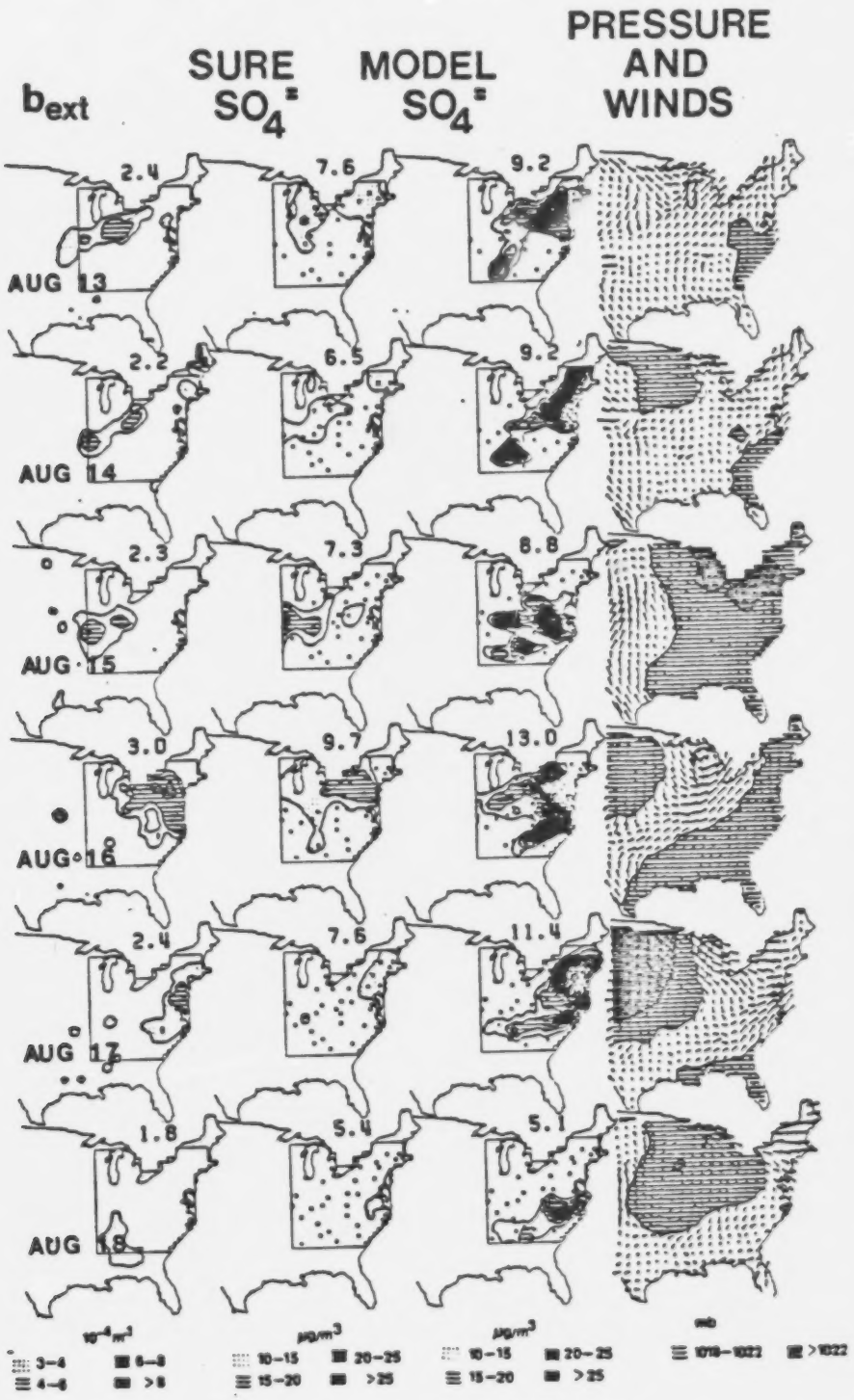

FIG. 9. As in Fig. 7 except for 13–18 August 1977.

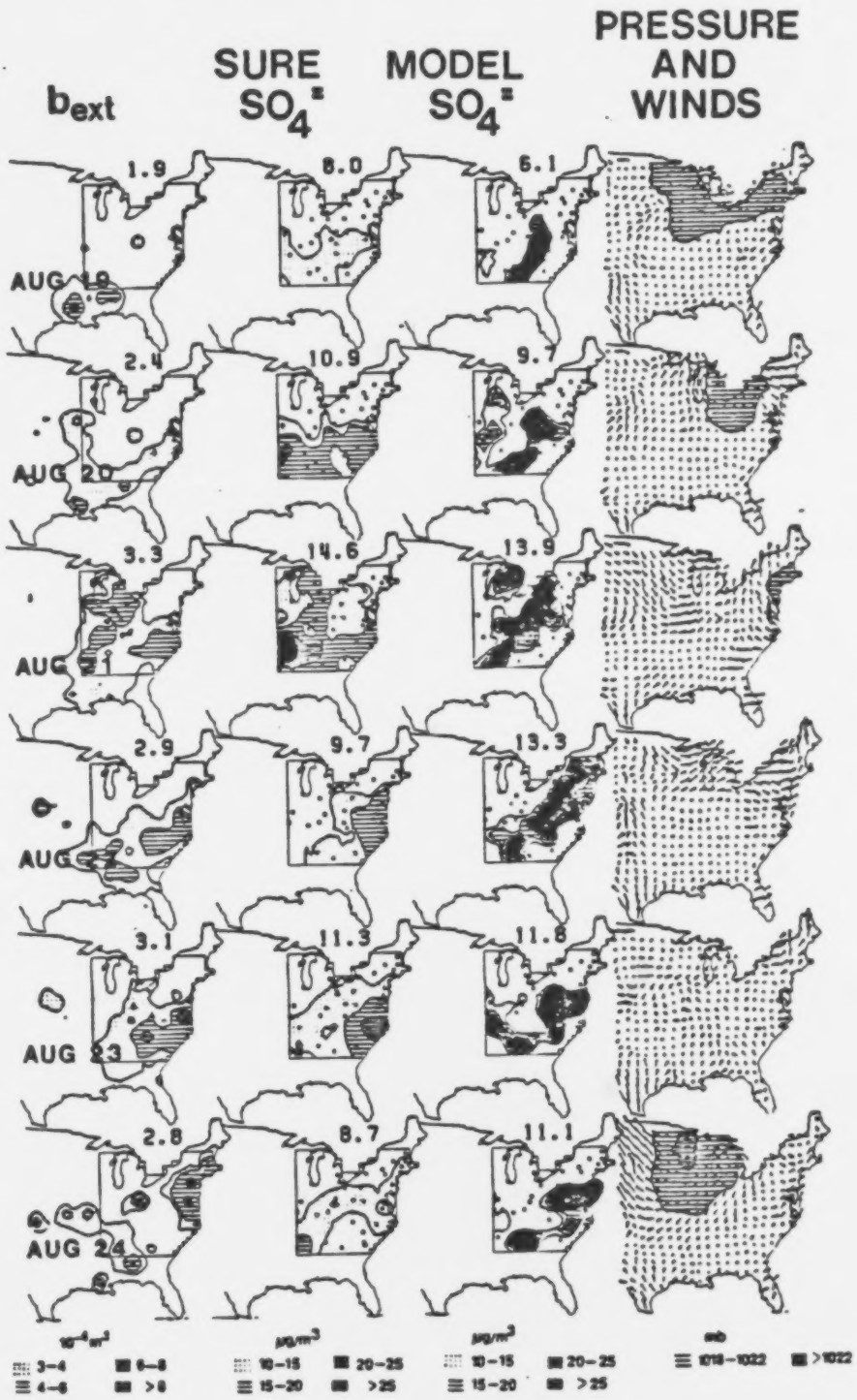

FIG. 10. As in Fig. 7 except for 19–24 August 1977.

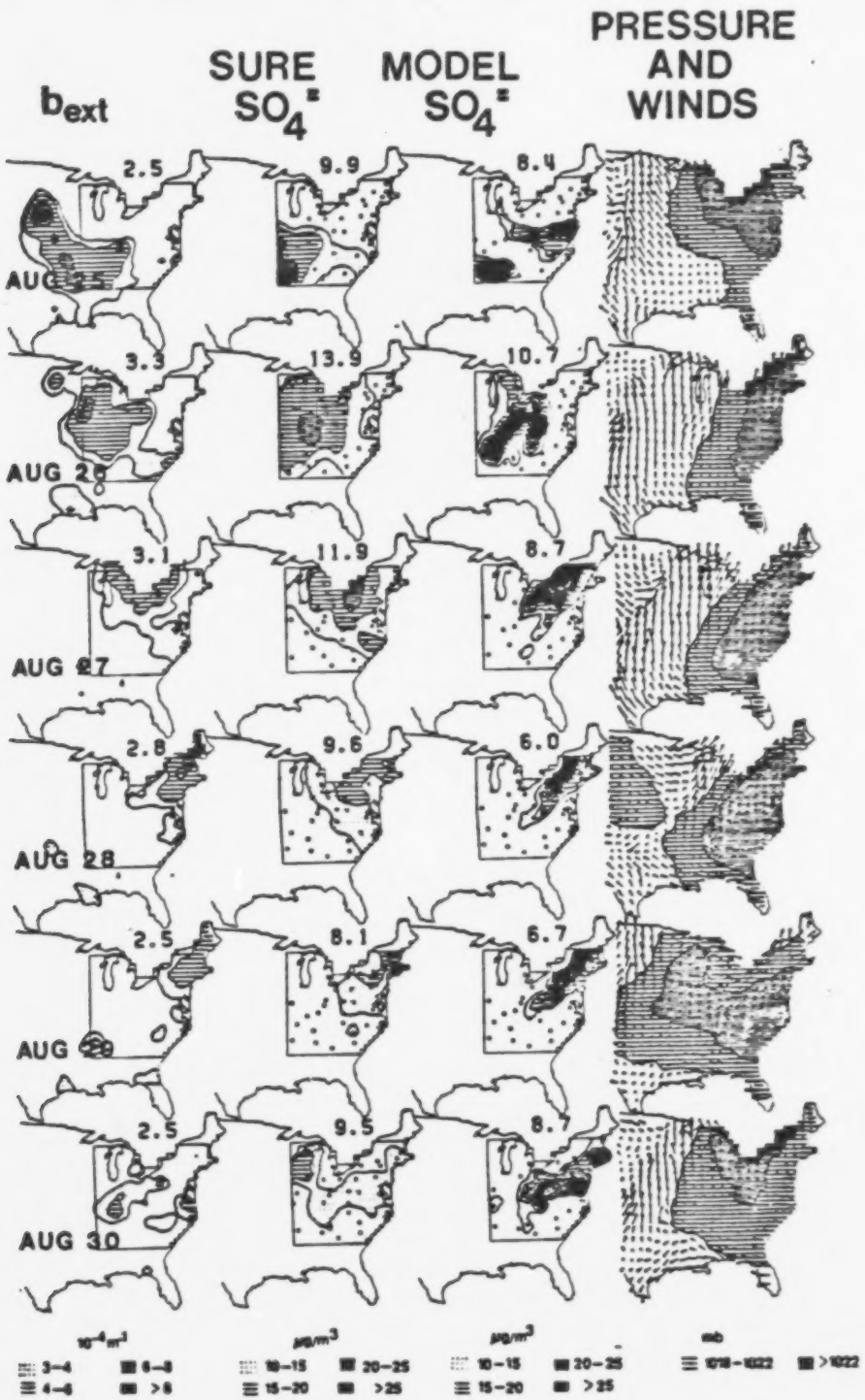

FIG. 11. As in Fig. 7 except for 25–30 August 1977.

such approaching high pressure systems move the emissions from the Ohio River Valley region first to the south and then to the west, markedly increasing their residence time over the United States. From the 26th to the end of the month, the high-pressure system became stationary over the eastern seaboard, resulting in the swift northeasterly transport of the emissions accumulated in the Midwest. By 30 August, the average sulfate level declined to about 9.5 $\mu g\ m^{-3}$ from a high of 13.9 $\mu g\ m^{-3}$ on 26 August.

The comparison of measured sulfate, observed haziness and simulated sulfate reveals an unexpectedly good spatial correspondence between daily maps of sulfate and visibility reduction during August 1977. The spatial correspondence between measured and simulated $SO_4^=$ can only be considered as fair. Major synoptic events, such as large-scale stagnations or strong regional ventilation on the backside of high-pressure systems, were adequately simulated. On 12 out of 31 days, "better than expected" agreement is shown, in that calculated and measured high concentration regions were within ~200 km of each other. Another 12 days show "about as expected" agreement, when the measured and simulated high concentrations were within the same general area of the eastern United States but deviated by 200–500 km. The agreement is characterized as "disappointingly poor" on seven (23%) of the days, when high $SO_4^=$ levels appeared either in the observed or simulated fields without an appropriate match in the other set.

The causes of poor performance cannot be quantified. Some of the inadequacy must be attributed to the wind fields. Large-scale lifting of near surface layers above the mixing layers during frontal passages and the effects of strong nocturnal shear are beyond our resolution. It also is likely that simulated dispersion is inadequate, since simulated sulfate distribution generally displays much steeper spatial gradients than the measured values. Episodic wet removal and transformation in cloud systems are potential causes of mismatch. It would be desirable to know whether other long-range transport models applied to the eastern United States (e.g., Henmi and Reiter, 1978; McNaughton, 1980) also show major discrepancies with *daily* SURE sulfate data.

b. *Daily spatial averages*

Another approach for the testing of agreement between $SO_4^=$, b_{ext} and simulated $SO_4^=$ is to examine their spatial averages within the SURE region from day to day. The daily variation of these quantities, Fig. 12, shows that in August 1977 average sulfate varies between 5.4 and 14.6 $\mu g\ m^{-3}$, light extinction coefficient between 1.8 (13.3 mi visual range) and $3.3 \times 10^{-4}\ m^{-1}$ (7.3 mi). The covariation of $SO_4^=$ and b_{ext} averages is rather striking. The least-squares-regression equation is $b_{ext} = 0.15[SO_4^=] + 1.2$, with correlation coefficient $r = 0.84$. The offset of $b_{ext} = 1.2$ is in part due to the fact that visual range > 12–20 mi is not resolved over the eastern United States. The regression implies that 70% of the b_{ext} variance could be explained by $SO_4^=$. It is important to recognize, however, that such a high correlation in this context does not establish a cause-effect relationship: when $SO_4^=$ concentration is high over the eastern United States, it is likely that all other air pollutants also are accumulated, and their contribution is statistically incorporated into the apparent effect of sulfate.

The Monte Carlo simulated daily average sulfate concentration shows a similar pattern to those of measured $SO_4^=$ and b_{ext}. The model correlations with

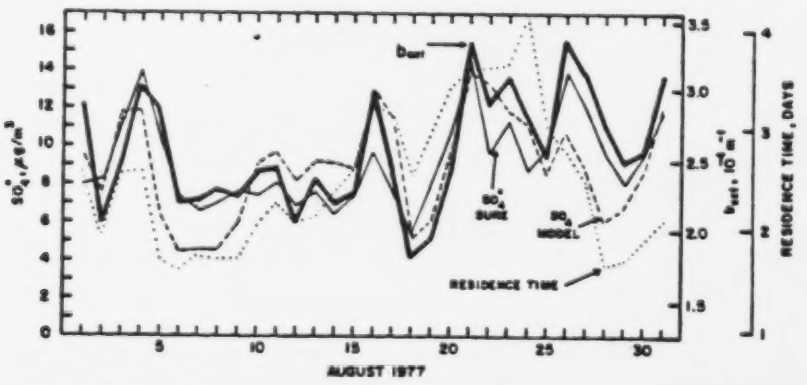

FIG. 12. Daily spatial averages within the SURE region of SURE sulfate (thin line), b_{ext} (thick line) and model sulfate (dashed line). Model sulfate scale assumes 1100 m scale height. The dotted trace is proportional to the number of conservative quanta from a uniform emission grid remaining within the eastern United States, which defines a regional residence time for the airmass.

SURE $SO_4^=$ and b_{ext} are 0.63 and 0.67, respectively. Thus the results indicate that the simulation succeeds at least as well as a *visual range* model. The key features of the daily average sulfate variations are reflected in the simulation: the accumulation and clearing from 2–6 August; the strong ventilation on 18 August, followed by the accumulation between 18–21 August. However, there are also strong deviations between the predicted and observed sulfate levels on 4–9, 14–17, 22–24 and 26–28 August. The ratio of predicted to observed spatial average sulfate varies from 0.6 to 1.5 with a mean of 1, with extended periods of consistent over- and underestimation.

c. *Monthly average maps*

The August 1977 monthly average concentration fields (Fig. 13) reveal that the highest measured $SO_4^=$ levels were in Pennsylvania, averaging in excess of 12 $\mu g\ m^{-3}$; the northeastern quadrant east of Missouri and north of Georgia shows $>8\ \mu g\ m^{-3}$. The lowest averge visual range (<8.5 mi) is noted for Ohio, Pennsylvania and the Boston-Washington megalopolis. Possibly in the eastern megalopolis region compounds other than sulfate contribute appreciably to visibility degradation. The average visual range is <10 mi in Louisiana, Mississippi and Alabama, but the lack of SURE stations there prevents $SO_4^= - b_{ext}$ comparison. The monthly average simulated $SO_4^=$ shows highest density around Pennsylvania-West Virginia, with a smaller high-density region occurring in Tennessee and northern Alabama (Fig. 13c).

The measured and simulated sulfate density show two discrepancies. The simulated $SO_4^=$ pocket in Tennessee does not appear in the measured data, which may be due either to inadequacies of the model or due to the incomplete spatial coverage of the SURE data base. Second, the SURE data base indicates only about a factor of two variation of $SO_4^=$ (6–12 $\mu g\ m^{-3}$) within the region, while simulated contours predict a factor of 5–10 variation. It should be noted that other model predictions of the same time period as part of Project MAP3S (McNaughton, 1980) also show a good match to SURE data in Pennsylvania, but, like the current Monte Carlo model, substantially underestimate the concentrations at the eastern and southern boundaries of the region. Both natural sources and man-made sources outside of the modeled region could explain the higher than modeled $SO_4^=$ at the region boundaries.

5. Discussion and conclusions

One important use of such modeling is to provide a method for examining the relative importance of the physical and chemical processes involved in producing regional scale pollution. McNaughton (1980), for example, has established the apparent insensitivity of his regional-scale model to diurnal variations in the rates of transformation and removal.

Effects of emission field and kinetic specification in the Monte Carlo simulation have been examined in terms of correlation of daily spatial averages (Table 2). The simulation was run for August 1977 with a spatially uniform emission grid of 204 quanta covering the United States east of the Mississippi River. With no kinetics imposed, the number of quanta remaining within the eastern United States defines the regional airmass residence time, (number of quanta/emission rate), which is plotted as a dotted trace in Fig. 12. The correlation coefficient $r = 0.96$ between the two residence time estimates, arising from the uniform grid and the SO_2 emission field of

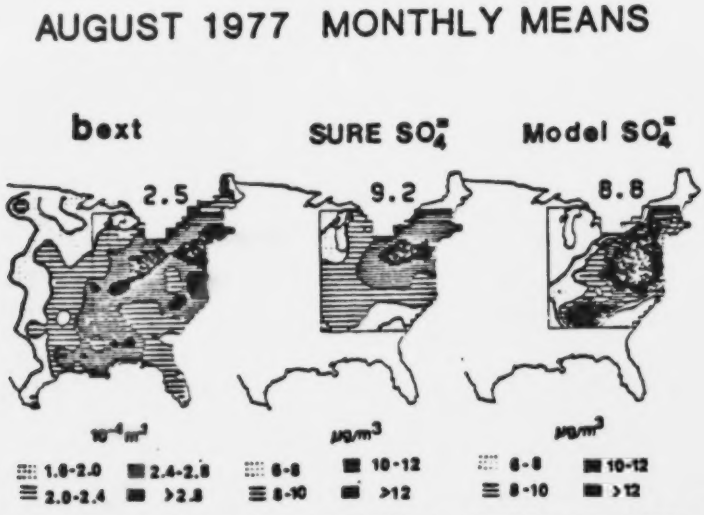

FIG. 13. August 1977 average distribution of midday b_{ext}, SURE $SO_4^=$ and model $SO_4^=$.

TABLE 2. Correlations of daily spatial averages.

	Uniform grid, no kinetics	EPA grid, no kinetics	EPA grid, model SO_2	EPA grid, model $SO_4^=$	SURE data, $SO_4^=$
Uniform grid, no kinetics	1.00				
EPA grid, no kinetics	0.96	1.00			
EPA grid, model SO_2	0.68	0.80	1.00		
EPA grid, model $SO_4^=$	0.70	0.89	0.84	1.00	
SURE data, $SO_4^=$	0.38	0.57	0.40	0.63	1.00
NWS data b_{ext}	0.40	0.62	0.36	0.67	0.84

Fig. 1d, indicates a weak dependence of the average levels on emission location. The SO_2 emission field yields a high correlation ($r = 0.89$) between average residence time and simulated $SO_4^=$; the agreement between SURE $SO_4^=$ and model output decreases only from $r = 0.63$ to $r = 0.57$ if the residence time is used in place of predicted sulfate concentration. Thus, between the extremes of conservative emissions of $SO_4^=$ (i.e., residence time alone) and the kinetic model described in the Appendix, the daily spatial average simulation appears to be surprisingly insensitive to choice of kinetic parameters. Thus, the variability of the daily average $SO_4^=$ concentration as obtained from the full kinetic $SO_4^=$ model is nearly proportional to the variability in airmass residence time. This implies that regional-scale episodes of $SO_4^=$ and light extinction coefficient can be attributed to poor regional ventilation without the need to invoke episodic $SO_4^=$ formation rates.

This work lead to the following conclusions:

- Daily simulation of regional sulfate concentration and light extinction coefficient is meaningful.
- High concentrations (episodes) over the entire SURE region are primarily due to high airmass residence time.
- The light extinction coefficient is a reasonable surrogate for $SO_4^=$ concentration; conversely, a $SO_4^=$ model is a reasonable surrogate for a visual-range model.

Acknowledgments. This work was supported by EPA Grants R806606 and R806548. Dr. Charles Hakkarinen of EPRI provided invaluable assistance in examination of the SURE and b_{ext} data. Mr. Dale Coventry of EPA-RTP provided the trajectory computations using the Heffter model. We wish to thank Ms. Jan Holloway of CAPITA for preparing the maps and assisting throughout. The kind permission of EPRI to obtain and use the SURE data is gratefully acknowledged.

APPENDIX

In analytic form, the mass budget equations within each emission quanta (well-mixed boxes) are of the form

$$\frac{dS}{dt} = -(k_t + k_r)S, \quad S(0) = 1 \; [S = SO_2],$$

$$\frac{dA}{dt} = k_t S - k_d A, \quad A(0) = 0 \; [A = SO_4^=],$$

$$\frac{dD}{dt} = k_r S, \quad D(0) = 0 \; [D = \text{deposited } SO_2],$$

$$\frac{dW}{dt} = k_d A, \quad W(0) = 0 \; [W = \text{deposited } SO_4^=],$$

where k_t, k_r, k_d correspond to the rate constants for SO_2 to $SO_4^=$ transformation, SO_2 deposition and $SO_4^=$ deposition, respectively. The solutions are

$$S(t) = \exp[-(k_t + k_r)t],$$

$$A(t) = \frac{k_t}{k_t + k_r - k_d}\{\exp(-k_d t) - \exp[-(k_t + k_r)t]\},$$

$$D(t) = \frac{k_r}{k_t + k_r}\{1 - \exp[-(k_t + k_r)t]\},$$

$$W(t) = \frac{k_t}{k_t + k_r}\{1 - \exp[-(k_t + k_r)t]\} - A(t).$$

For $k_d = k_t + k_r$, $A(t) = tk_t \exp(-k_d t)$

$SO_4^=$ peaks at time $T = \dfrac{\ln(k_t + k_r) - \ln k_d}{k_t + k_r - k_d}$.

The current values of $k_t = 0.013\ h^{-1}$, $k_r = 0.035\ h^{-1}$ and $k_d = 0.015\ h^{-1}$ lead to a peak $SO_4^=$ mass fraction of 16% at 1.5 days (35 h) after emission. Decay to $1/e$ of maximum sulfate mass occurs at five days (126 h) after emission, or 91 h after the $SO_4^=$ maximum.

REFERENCES

Alsmiller, F. S., R. G. Alsmiller, H. W. Bertini and C. L. Begovich, 1979: Monte Carlo simulation of turbulent atmospheric transport and comparisons with experimental data. *J. Appl. Meteor.*, **18**, 17–26.

Bonner, W. D., S. Esbesen and R. Greenberg, 1968: Kinematics of the low-level jet. *J. Appl. Meteor.*, **7**, 339–347.

Counihan, J., 1975: Adiabatic atmospheric boundary layers: A review and analysis of data from the period 1880–1972. *Atmos. Environ.*, **9**, 871–905.

Covert, D. S., R. J. Charlson and N. C. Ahlquist, 1972: A study

of the relationship of chemical composition and humidity to light scattering by aerosols. *J. Appl. Meteor.*, 11, 968–976.

Eliassen, A., 1978: The OECD study of long-range transport of air pollutants: Long-range transport modeling. *Atmos. Environ.*, 12, 479–487.

Hall, C. D., 1975: The simulation of particle motion in the atmosphere by a numerical random-walk model. *Quart. J. Roy. Meteor. Soc.*, 101, 235–244.

Heffter, J. L., A. D. Taylor and G. J. Ferbert, 1975: A regional-continental scale transport, diffusion and deposition model. NOAA Tech. Memo. ERL ARL-50, 26 pp.

Henmi, T., and E. R. Reiter, 1978: Regional residence time of sulfur dioxide over the eastern United States. *Atmos. Environ.*, 12, 1489–1495.

Hidy, G. M., P. K. Mueller and E. Y. Tong, 1978: Spatial and temporal distribution of airborne sulfate in parts of the United States. *Atmos. Environ.*, 12, 735–752.

International Symposium on Sulfur in the Atmosphere Workship Reports, 1978: *Atmos. Environ.*, 12, 7–17.

Maul, P. R., 1978: The effect of the turning of the wind vector with height on the ground level trajectory of a diffusing cloud. *Atmos. Environ.*, 12, 1045–1050.

McNaughton, D. J., 1980: Initial comparison of SURE/MAP3S sulfur oxide observations with long-term regional model predictions. *Atmos. Environ.*, 14, 55–63.

Munn, R. E., and B. Bolin, 1971: Global air pollution—meteorological aspects: A survey. *Atmos. Environ.*, 5, 363–402.

Pack, D. H., G. J. Ferber, J. L. Heffter, K. Telegadas, J. K. Angell, W. H. Hoecker and L. Machta, 1978: Meteorology of long-range transport. *Atmos. Environ.*, 12, 425–444.

Perhac, R. M., 1978: Sulfate regional experiment in northeastern United States: The 'SURE' program. *Atmos. Environ.*, 12, 641–647.

Samson, P. J., 1978: Ensemble trajectory analysis of summertime sulfate concentrations in New York. *Atmos. Environ.*, 12, 1889–1893.

——, 1980: . Trajectory analysis of summertime sulfate concentrations in the northeastern United States. *J. Appl. Meteor.* 19, 1382–1394.

Smith, F. B., and G. H. Jeffrey, 1975: Airborne transport of sulfur dioxide from the U.K. *Atmos. Environ.*, 9, 643–659.

Smith, T. B., D. L. Blumenthal, J. A. Anderson and A. H. Vanderpol, 1978: Transport of SO_2 in power plant plumes: Day and night. *Atmos. Environ.*, 12, 605–611.

U.S. Department of Commerce, 1975: *Federal Meteorological Handbook No. 1, Surface Observations*. Govt. Printing Office, Washington, DC, 309 pp. [GPO C1.8-4:1/CH3].

U.S. EPA, 1976: National Emissions Report (1973). National Emissions Data System (NEDS). EPA-450/2-76-007, U.S. Environmental Protection Agency, Research Triangle Park, NC. [NTIS-EP1,69;973].

Wolff, G. T., P. J. Lioy, R. E. Meyers and R. T. Cederwall, 1977: An investigation of long-range transport of ozone across the midwestern and eastern United States. *Atmos. Environ.*, 11, 797–802.